

# Spin exciton in a quantum dot with spin-orbit coupling at high magnetic field

P.Lucignano<sup>1,2</sup>, B.Jouault<sup>3</sup>, and A.Tagliacozzo<sup>1,2</sup>

<sup>1</sup> *Coherentia-INFM, Unità di Napoli*

<sup>2</sup> *Dipartimento di Scienze Fisiche Università di Napoli "Federico II "*  
*Monte S. Angelo - via Cintia, I-80126 Napoli, Italy and*

<sup>3</sup> *GES, UMR 5650, Université Montpellier II*  
*34095 Montpellier Cedex 5, France*

(Dated: December 30, 2021)

Coulomb interactions of few ( $N$ ) electrons confined in a disk shaped quantum dot, with a large magnetic field  $B = B^*$  applied in the  $z$ -direction (orthogonal to the dot), produce a fully spin polarized ground state. We numerically study the splitting of the levels corresponding to the multiplet of total spin  $S = N/2$  (each labeled by a different total angular momentum  $J_z$ ) in the presence of an electric field parallel to  $B$ , coupled to  $S$  by a Rashba term. We find that the first excited state is a spin exciton with a reversed spin at the origin. This is reminiscent of the Quantum Hall Ferromagnet at filling one which has the skyrmion-like state as its first excited state. The spin exciton level can be tuned with the electric field and infrared radiation can provide energy and angular momentum to excite it.

PACS numbers: PACS numbers:73.21.La,73.23.-b,78.67.Hc

## I. INTRODUCTION

Quantum dots are semiconductor devices in which electrons are confined to a small area within a two dimensional electron gas by properly biasing metal gates added to the structure<sup>1,2</sup>. In an isolated quantum dot (QD) the confining potential gives rise to quantized single particle energy levels. However, electron-electron interaction determines the dot properties. In dots having a diameter of  $\sim 100\text{nm}$ , the level spacing and the Coulomb energy are of the order of  $\sim 1\text{meV}$  and most charging properties can be included within the Hartree-Fock ( $H-F$ ) approximation, just like in atoms. Correlation effects do not significantly alter the charging properties, but may strongly influence the spin properties of the confined electrons. One striking evidence of this is the fact that Hund's rule, which is typical of atoms, is often satisfied in dots<sup>3</sup>. However, the reduction of the energy scale by a factor of  $10^{-3}$  with respect to atoms, enhances the sensitivity of the electrons in the dot to an external magnetic field. In this paper we discuss the spin properties of an isolated vertical QD in presence of a magnetic field  $B$  in the  $z$ -direction, orthogonal to the dot disk (cylindrical symmetry is assumed). We also include the spin orbit coupling ( $SO$ ) induced by an electric field along  $z$ .

In the cylindrical geometry, orbital effects are dominant<sup>4</sup>. Indeed Zeeman spin splitting does not drive any spin polarization in these systems and can be often ignored<sup>5</sup>. However correlations combine orbital and spin effects together and can be probed by magnetoconductance measurements in a pillar configuration<sup>6,7</sup>. Spin properties are quite relevant to conductance, in view of the possibility of spin blockade<sup>8,9</sup>, Kondo effect<sup>10,11</sup>, or Berry phase induced tuning<sup>12</sup>.

Quantum numbers labeling the dot energy levels are the number of electrons  $N$ , the total orbital angular momentum along  $z$ ,  $M$ , the total spin  $S$  and the

$z$ -component of the spin  $S_z$ . By increasing the magnetic field  $B$ , both  $M$  and  $S$  increase. Finally, at  $B = B^*$ , a fully spin polarized ( $FSP$ ) state is reached. The increasing of the total spin  $S$  was measured in a dot with about 30 electrons, a striking evidence of e-e correlations<sup>13</sup>. While, in the absence of interactions, the density of the  $FSP$  state becomes uniform over the dot area, which is contracted to a minimum, in the real case, the e-e interaction tends to reduce the density at the center of the disk, by compressing the electrons at the dot edge (see Fig.2 [middle panel]). By further increasing  $B$ , the electron density reaches a maximum value. The dot becomes a so called "Maximum Density Droplet" ( $MDD$ )<sup>14</sup>. For larger  $B$  values, the  $FSP$  state is disrupted: the dot density reconstructs i.e. an annular local maximum of the density is produced at the edge of the dot<sup>15</sup> with breaking of azimuthal symmetry at the edge (de Chamon-Wen phase<sup>16</sup>).

Various numerical calculations<sup>17</sup> have investigated these subsequent electronic transformations which appear as crossing of levels with different quantum numbers.  $H-F$  calculations are known to incorrectly favor spin-polarized states<sup>18</sup>. Spin density functional calculations have been performed for dots including a larger number of electrons<sup>19</sup>. The density functional approach, with a good choice of the parameters of the potentials, can reach a significative agreement with the experiments, but it may introduce uncontrolled approximations. When the electron density is reduced, a Wigner molecule can be formed. Recently, this broken symmetry state has been studied in the absence of an external magnetic field, using Quantum Monte Carlo simulations, with a multilevel blocking algorithm which is free of the sign problem<sup>20</sup>.

In this work, we use exact diagonalization for few electrons with azimuthal symmetry<sup>9</sup> to discuss the spectral properties of the  $FSP$  dot which is stabilized by the Coulomb interaction. Electrons are confined to a two-

dimensional  $(2-d)$  disk by a  $2-d$  parabolic potential and interact via the full Coulomb repulsion whose strength is parametrized by  $U = e^2/\kappa l$ . Here  $l$  is the magnetic length due to the parabolic confinement in presence of a field  $B$  along  $z$  and  $\kappa$  is the static dielectric constant. The confinement of the electrons in the  $x-y$  plane implies the presence of an electric field in the  $z$ -direction, provided by the band bending of the heterostructure. This gives rise to the so called *SO* Rashba term<sup>21</sup>, which can be enhanced even further in a non-linear conductance measurement, when an extra bias voltage  $V_{sd}$  is applied to the contacts of a vertical structure.

In the presence of *SO*,  $J_z = M + S_z$  becomes the good quantum number. The *FSP* ground state (GS) has  $J_z = N(N-1)/2 + S$  ( $J_z = 25/2$  for  $N = 5$ ), while the first excited state (denoted as *SKD* state in the following) has  $J_z = N(N-1)/2 + S - 1$  ( $J_z = 23/2$  for  $N = 5$ ). The charge density is rather insensitive to the *SO* coupling,  $\alpha$ . However, we show that the *SO* interaction couples the spin polarization to the orbital motion determining the spin properties of the GS and the first excited states in a surprising way. Indeed, by increasing  $\alpha$ , the expectation value of the spin density of the GS, which was originally oriented in the  $z$ -direction, acquires a component in the dot plane, because the minority spin density is increased and pushed from the center of the dot outward. Moreover the combined effect of  $U$  and  $\alpha$  deforms substantially the spin density of the *SKD*. A sharp minority spin polarization is present close to the dot center. The reversal of the spin polarization at the origin in the *SKD* state w.r. to the *FSP* GS leads to an extra node in the spin density.

This situation is reminiscent of the case of the Quantum Hall Ferromagnet (*QHF*)<sup>22</sup> close to filling one. In that case, a true magnetic ordering is achieved, which is characterized by full spin polarization in the GS and by a topologically constrained first excited state, the Skyrmion (*SK*) state, with reversal of the spin at the origin, first studied in the  $O(3)$  non linear  $\sigma$  model (*NLSM*) in  $2-d$  dimensions<sup>23,24</sup>. In Section V, we elaborate on the analogies and differences between the *FSP* dot and the *QHF*. In the *QHF* a topological quantization of charge occurs. By contrast the *SKD* state has no topological features, because the geometrical compactification procedure described in Subsection V.A cannot take place. We refer to the *SKD* state as a “spin exciton” because there is some piling up of the charge at the center of the dot w.r. to the GS, together with the reversal of the spin polarization there.

The paper is organized as follows:

In Sect. II we report our results of numerical diagonalization with the Lanczos algorithm for a dot with five electrons ( $N = 5$ ) close to the *FSP* state, in the absence of *SO* coupling.

In Sect. III we derive the *SO* matrix elements in the  $2-d$  harmonic oscillator basis and discuss how the *SO* coupling modifies the lowest lying energy levels.

In Sect. IV we show the spin and charge density of the

lowest lying  $J_z$  multiplet when the *FSP* state is achieved.

In Sect. V we summarize the features of the *SK* state in the *QHF* and compare these with the ones of the *SKD* state in a dot with *SO* coupling.

A brief summary and some conclusions are outlined in Sect. VI.

There is evidence of skyrmion excitations in *GaAs*  $2-d$  electron gas systems close to filling one by magnetoabsorption spectroscopy<sup>25</sup>. A sharp absorption line could be found in exciting dots to the *SKD* state, by transferral of energy and angular momentum with circularly polarized light. This amounts to adding a spin exciton to the dot.

## II. FSP STATE AND DOT RECONSTRUCTION

We consider  $N = 5$  electrons confined in two dimensions (spanned by the  $(\rho, \varphi)$  coordinates) by a parabolic potential of characteristic frequency  $\omega_d$ . This is a model for an isolated disk shaped QD. A magnetic field  $B$  orthogonal to the disk is measured in units of  $\hbar\omega_c$  (*meV*), where  $\omega_c$  is the cyclotron frequency. In the absence of spin orbit coupling, the single particle states  $\phi_{nm}$  are the eigenfunctions of the  $2-d$  harmonic oscillator with frequency  $\omega_o = \sqrt{\omega_d^2 + \frac{\omega_c^2}{4}}$ . They are labeled by  $n, m$  (with  $n \in (0, 1, 2, 3, \dots)$  and  $m \in (-n, -n+2, \dots, n-2, n)$ ).  $m$  is the angular momentum in the  $z$  direction:

$$\phi_{nm} = \frac{e^{im\varphi}}{l\sqrt{\pi}} R_{n|m|}(t) = C_{nm} \frac{e^{im\varphi}}{l\sqrt{\pi}} e^{-\frac{\rho^2}{2l^2}} \left(\frac{\rho}{l}\right)^{|m|} L_{\frac{n-|m|}{2}}^{|m|} \left(\frac{\rho^2}{l^2}\right). \quad (1)$$

Here  $L_n^\alpha(t)$  (with  $t = \rho^2/l^2$ ) is the generalized Laguerre polynomial with  $n \geq 0$ <sup>26</sup>,  $l = \sqrt{\hbar/m^*\omega_o}$  is the characteristic length due to the lateral geometrical confinement in the dot inclusive of the  $B$  field effects and

$C_{nm} = \left[ \frac{(\frac{n-|m|}{2})!}{(\frac{n+|m|}{2})!} \right]^{\frac{1}{2}}$  is a normalization factor.

The corresponding single particle energy levels are

$$\epsilon_{n,m} = (n+1)\hbar\omega_o - \frac{m}{2}\hbar\omega_c. \quad (2)$$

In the absence of both interaction and magnetic field, the lowest lying single particle states are occupied with the minimum spin. The GS Slater determinant is sketched pictorially in Fig. 1a, where energy is intended on the vertical axis. Each box represents a single particle state labeled by  $n, m$  and arrows represent electron occupancy with spin projection along the quantization axis. We have performed exact diagonalization of this system including Coulomb interaction between the electrons. The matrix elements of the unscreened Coulomb interaction use the single particle basis set, up to 28 orbitals. They can be calculated analytically and are parametrized by the strength of the interaction  $U$ . Our calculation is limited to very small particle numbers ( $N < 7$ ), because the

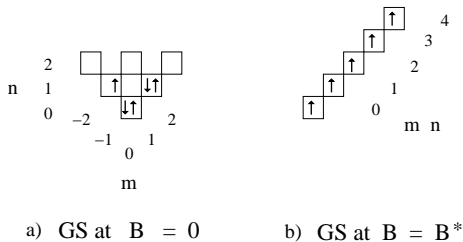


FIG. 1: Slater determinants quoted in the text are depicted. Quantum numbers are  $N = 5$ ,  $S = 1/2$  for the state at  $B = 0$  [a)] and  $S = 5/2$  for the state at  $B = B^*$ , the magnetic field value at which the maximum of  $S$  is achieved [b)].

truncation of the Hilbert space influences the results for larger  $N$ . However, our convergency checks show that the numerical errors proliferate only at higher energies. In particular they affect the reliability of the level spin degeneracy. In any case, numerical errors are quite small if  $N = 5$ . In Fig.2 [left panels], we show the lowest lying total energy levels at fixed angular momentum  $M$ , versus  $M$ , for  $U = 13 \text{ meV}$ . Magnetic field is  $B = 5 \text{ meV}$  [top],  $B = B^* = 7 \text{ meV}$  [middle],  $B = 11.5 \text{ meV}$  [bottom]. At each  $M$ , the spin degeneracy is marked by dashes of different length: short dashes for  $S = 1/2$  (doubly degenerate level), medium dashes for  $S = 3/2$  (fourfold degeneracy) and long dashes for  $S = 5/2$  (sixfold degeneracy). On the r.h.s. of the picture the radial charge density of the corresponding GS is plotted *vs* distance  $r$  from the dot center. Fig.2 ([left panels]) shows the crossing of levels with increasing  $B$ . Electron-electron correlations imply that when  $M$  increases,  $S$  also increases. At  $B = B^* = 7 \text{ meV}$  the spin  $S$  reaches its maximum value  $S = N/2$ . The largest contribution to the GS wavefunction is given by the Slater determinant depicted in Fig.1b) corresponding to  $M = \sum_0^{N-1} m = 10$ . We concentrate on the state at  $B = B^*$ , the *FSP* GS. This corresponds to the “maximum density droplet” state discussed in the literature<sup>14</sup>. Qualitatively we can say that at  $B = B^*$  the dot attains its smallest radius. As can be seen from the GS charge density, further increase of  $B$  leads to the so called reconstruction of the charge density of the dot. For  $B > B^*$ , the  $M$  of the GS increases further, but  $S$  is no longer at its maximum. In the bottom panel of Fig.2 it is shown that at  $B = 11.5 \text{ meV}$  the GS energy is now achieved for  $M = 13$  with a doublet ( $S = 1/2$ ) state. The corresponding charge density of the dot, as depicted on the r.h.s, is strongly modified close to the edge<sup>15</sup>: it displays a node followed by an extra non zero annulus at a larger distance. In view of the fact that our expansion of the wavefunction only includes rotationally invariant components, the breaking of the azimuthal symmetry is impossible. By contrast this is found to occur in density functional calculations and the corresponding GS is referred to as the de Chamou-Wen phase<sup>16</sup>. The GS at  $B = B^*$  can be compared with a *FSP* quantum Hall state of an extended disk in the absence of lateral confinement (Quantum Hall Ferro-

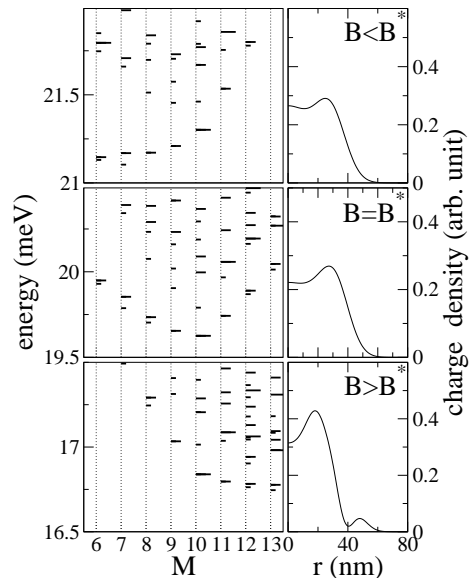


FIG. 2: Energy levels without *SO* coupling for the dot with  $N = 5$  electrons at  $U = 13 \text{ meV}$  and  $\omega_d = \text{meV}$ . Magnetic field values are: (in units of  $\hbar\omega_c$ ):  $B = 5 \text{ meV}$  [top],  $B = B^* = 7 \text{ meV}$  [middle],  $B = 11.5 \text{ meV}$  [bottom]. The total  $M$  is on the  $x$  axis. The levels are drawn with short, medium or long dashes, depending on the total spin :  $S = 1/2, 3/2, 5/2$

magnet (QHF) at filling one). Fig. 1b) recalls the occupancy of the lowest Landau level (LLL) up to a maximum  $m = N - 1$ , except for the fact that in our case the single particle levels corresponding to the LLL are not all degenerate in energy. In the language of the quantum Hall effect the unperturbed levels are:

$$\epsilon_{\nu,m} = (2\nu + |m| + 1)\hbar\omega_o - \frac{m}{2}\hbar\omega_c \quad (3)$$

where  $\nu = (n - |m|)/2$ . LLL is for  $\nu = 0$  and  $m \geq 0$ . The Slater determinant of Fig.1b) has a charge density which is flat as a function of the radius  $r$ , up to the disk edge, where it rapidly falls down to zero. In our case this feature is lost because of the presence of  $U$ , together with the fact that the number of electrons is small. We will better discuss the comparison of the *FSP* GS with the *QHF* in Section V.

### III. INCLUSION OF SPIN-ORBIT

We now add the spin orbit interaction to the *FSP* GS at  $B = B^*$ . This can be tuned by applying an electric field  $\mathbf{E}$  in the  $\hat{z}$  direction, which couples to the spin of the electrons in the dot with a term<sup>21</sup>:

$$H_{so} = \frac{\alpha}{\hbar} (\hat{z} \times \mathbf{p}) \cdot \vec{\sigma}. \quad (4)$$

Here  $\vec{\sigma}$  are the Pauli matrices,  $\alpha$  is the spin-orbit coupling parameter which is proportional to the electric field.  $\alpha$  will be measured in units of  $\text{meV} \cdot \text{\AA}$ . We now rewrite the

spin-orbit coupling term in a second quantized form. We denote the fermion operators associated to  $\phi_{nm}$  of Eq.(1)

by  $c_{nm\sigma}, c_{nm\sigma}^\dagger$  and we get:

$$H_{so} = \alpha \sum_{nm} \sum_{n'm'} \left\{ \langle n'm' | -(\frac{\partial}{\partial x} + i\frac{\partial}{\partial y}) | nm \rangle c_{n'm'\downarrow}^\dagger c_{nm\uparrow} + \langle n'm' | \frac{\partial}{\partial x} - i\frac{\partial}{\partial y} | nm \rangle c_{n'm'\uparrow}^\dagger c_{nm\downarrow} \right\}. \quad (5)$$

The integration over the azimuthal angle  $\varphi$  can be done analytically. This shows that the Hamiltonian can be rewritten in the following way:

$$H_{so} = \frac{\alpha}{l} \sum_{nn'} \sum_m \left( B_{n'm+1,nm} c_{n'm+1\downarrow}^\dagger c_{nm\uparrow} + A_{n'm-1,nm} c_{n'm-1\uparrow}^\dagger c_{nm\downarrow} \right) \quad (6)$$

with  $A_{n'm'nm} =$

$$\delta_{m'+1,m} \int_0^\infty dt R_{n'|m'}(t) (2\sqrt{t} \frac{\partial}{\partial t} + \frac{m}{\sqrt{t}}) R_{n|m}(t)$$

and  $B_{n'm'nm} =$

$$\delta_{m'-1,m} \int_0^\infty dt R_{n'|m'}(t) (2\frac{\partial}{\partial t} \sqrt{t} + \frac{m'}{\sqrt{t}}) R_{n|m}(t)$$

Here  $B_{nm,n'm-1} = A_{n'm-1,nm}^*$ , what implies that the hamiltonian is hermitian. It is clear that while  $s_z$  and  $m$  are no longer separately conserved, their sum  $j_z = s_z + m$  (with  $j_z$  half integer) is a good quantum number. We will denote the single particle basis that diagonalizes the  $SO$  term by  $w_{j_z}^\beta$  with  $\beta = p, m$ . The label  $\beta$  takes two possible values, say  $p, q$  and allows for conservation of the number of degrees of freedom.

The  $SO$  interaction lifts the spin degeneracy. In Fig.3 we show the splitting of the multiplet with  $N = 5$ ,  $S = 5/2$ ,  $M = 10$  at  $B = B^* = 7 \text{ meV}$  and  $U = 13 \text{ meV}$  vs the strength of the  $SO$  coupling  $\alpha$ . The strength of  $U$  is responsible not only for the fact that the GS belongs to this multiplet, but also for the ordering in energy of the sequence:  $J_z = 25/2, 23/2, 21/2, 19/2, 17/2, 15/2$  (from bottom to top). At small  $U$  values the sequence is  $J_z = 15/2, 17/2, 19/2, 21/2, 25/2, 23/2$ , as shown in Fig.4. With increasing of  $U$ , some level crossings occur. The ordering at three different values of  $U$  is magnified in the bottom panels of Fig.4. The case with  $U = 13 \text{ meV}$  is shown in the bottom right panel of Fig. 4. The lowest state in energy is for  $J_z = 25/2$  followed by  $J_z = 23/2, 21/2$  (almost degenerate with  $15/2$ ),  $15/2, 19/2, 17/2$ . At  $U = 13 \text{ meV}$  a sizeable gap is formed between the  $J_z = 25/2$  GS and the first excited state  $J_z = 23/2$  ( $SKD$ ). The other states of the multiplet are bunched together at higher energy. In this Section we focus on the  $U = 13 \text{ meV}$  case and discuss the charge density and the spin polarization density of the GS at

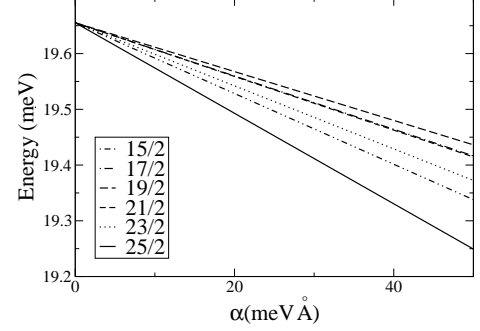


FIG. 3: Splitting of the lowest lying multiplet for  $N = 5, S = 5/2$  and  $M = 10$  vs strength  $\alpha$  of the  $SO$  interaction, at  $B = B^* = 7 \text{ meV}$ ,  $U = 13 \text{ meV}$  and  $\omega_d = 5 \text{ meV}$ . The levels are labeled by  $J_z$ .

$J_z = 25/2$ . The other states of the multiplet will be analyzed in Section IV.

As it appears from Fig. 5 [top panel], the charge density of the GS is only mildly changed when we increase the  $SO$  coupling. By contrast, the spin density is quite sensitive to the addition of  $SO$ , up to saturation. Now the  $z$ -component of the total spin is no longer a good quantum number and some admixture with down spin electrons appears. Indeed the role of the Rashba term is to rotate the average electron spin. In particular, down spin electrons are pushed away from the center of the dot, giving rise to the spin density components  $S_z(\vec{r})$  (orthogonal to the dot plane), and  $S_r(\vec{r})$  (in the plane of the dot), which are plotted in Fig.5 [middle and bottom panels, respectively]. It is remarkable that the spin density  $S_z(\vec{r})$  changes sign at the edge of the dot for large  $SO$  coupling. This is confirmed by a plot of the occupation numbers  $n_{nm\sigma} = \langle GS | c_{nm\sigma}^\dagger c_{nm\sigma} | GS \rangle$  with  $n = m$ . They are shown in Fig.6 for both  $N = 4$  and  $N = 5$  for comparison. Of course, the change of  $N$  would also imply an effective change of the confinement potential  $\omega_d$  (what we do not do). However, all what we want to show here is that our findings depend on the strength of  $B$  only, and not on the number of electrons being even or odd. A similar feature occurs in the de Chamoun-Wen phase, in the absence of  $SO$ : when crossing the edges, the spins tilt away from their bulk direction<sup>27</sup>.

The reversal of the spins in the tail at the dot boundary is a peculiarity of the Rashba interaction, but the spin/charge density is very small there and does not in-

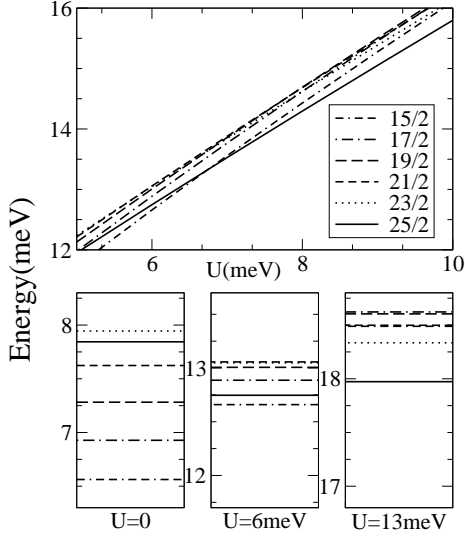


FIG. 4: Energy levels with  $B = 7$  meV,  $\omega_d = 5$  meV, and  $\alpha = 100$  meV  $\cdot$   $\text{\AA}$ , for different  $U$  values. In the upper panel we show the crossings that allow the *FSP* polarized state to be the ground state when  $U$  is large. Ordering of the levels is magnified in the bottom panels for three different  $U$  values.

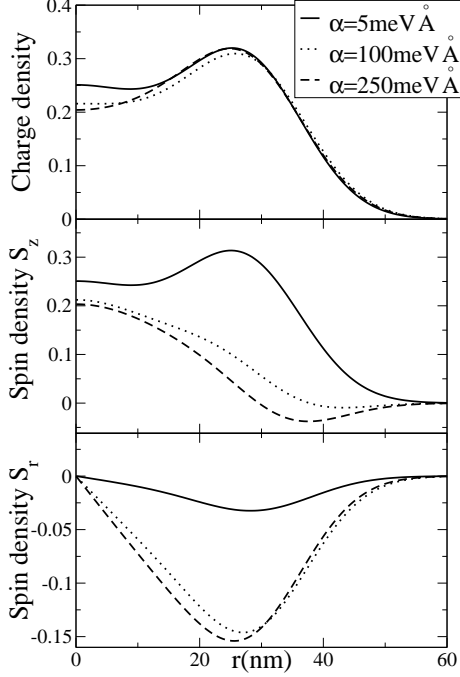


FIG. 5: Charge density, azimuthal spin density  $S_z$ , in plane spin density  $S_r$ , in the radial direction, in the GS ( $J = 25/2$ ) at various  $SO$  couplings:  $\alpha = 5, 100, 250$  meV  $\cdot$   $\text{\AA}$ . Here  $B = 7$  meV,  $U = 13$  meV and  $\omega_d = 5$  meV

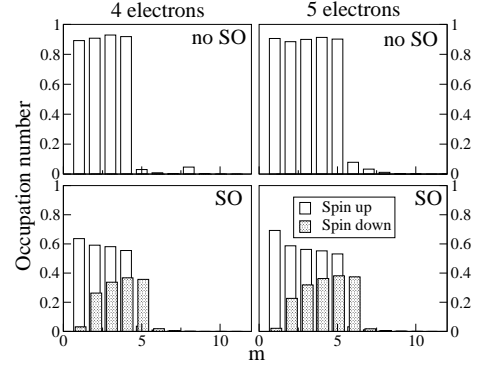


FIG. 6: Occupation numbers  $n_{n=m,m,\sigma}$  in the *GS* with  $N = 4(5)$  electrons (left(right)) without *SO* (top) and with *SO* ( $\alpha = 100$  meV  $\cdot$   $\text{\AA}$ ) (bottom). Other parameter values are  $B = 7$  meV,  $U = 13$  meV,  $\omega_d = 5$  meV. White bars refers to spin up, grey bars refer to spin down. The *FSP* GS of the dot with  $N = 4(5)$  electrons has total spin  $S = 2(5/2)$  and the  $z$ -component of the total angular momentum  $J_z = 8(25/2)$ .

fluence the dot properties.

#### IV. SPIN AND CHARGE DENSITY IN THE MULTIPLY $S = 5/2$ , $M = 10$

In the previous Section we have shown that at  $B = B^*$  the GS with  $N = 5$  electrons belongs to the  $S = 5/2$ ,  $M = 10$  multiplet. The *SO* coupling lifts its degeneracy as shown in Fig.3. The size of  $U$  strongly influences the energy of each state, by producing crossings of levels. At  $U = 13$  meV the lowest lying states with increasing energies are (see Fig.4[right bottom panel]):

$|GS\rangle \equiv |N = 5; S = 5/2, J_z = 25/2\rangle$ : this is the fully spin polarized GS.

$|SKD\rangle \equiv |N = 5; S = 3/2, J_z = 23/2\rangle$ : the ‘spin exciton’.

$|b\rangle \equiv |N = 5; S = 3/2, J_z = 15/2\rangle$ : this is a state higher in energy w.r. to  $|SKD\rangle$ .

This ordering of energy levels is again a consequence of Hund’s rule: lowest energy is for  $J_z = L_z + |S_z|$ , higher energy is for  $J_z = L_z - |S_z|$ . Besides affecting the energy of the states, the effect of  $U$  is to enhance the transfer of weight from the majority (“up”) to the minority (“down”) spin population. This is shown in Fig.7, where the occupation numbers  $n_{n=m,m,\sigma}$  are reported for the states  $|GS\rangle$ ,  $|SKD\rangle$  and  $|b\rangle$  for  $U = 0$  [left panels] and  $U = 13$  meV [right panels], respectively. A striking feature characterizes the spin densities of these states (see Fig.7, 8): the dominant spin density is reversed in the  $|b\rangle$  state, w.r.to the  $|GS\rangle$ . The state  $|SKD\rangle$ , which is the first excited state, interpolates between the two. Spin occupancy is not significantly modified for larger  $r$ .

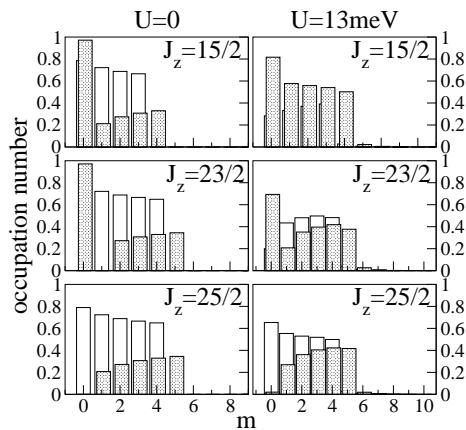


FIG. 7: The occupation numbers  $n_{n=m,m,\sigma}$  in the state at  $J_z = 15/2, 23/2, 25/2$  for small  $U$  [left], and large  $U$  [right]. White bars refers to spin up, grey bars refers to spin down. We stress that at  $U = 0$  the ordering of the levels, corresponding to the three panels on the left is changed w.r. to the ones on the right ( $U = 13 \text{ meV}$ ). (see Fig. 4 [bottom panels]).

While at  $U = 0$  the flipping of the spin at the origin w.r. to the GS is full, in the interacting case some up-spin is left at the center. This allows for a smoother radial dependence of the spin and charge density expectation values. Eventually, this is the reason why this state turns out to be the lowest excited state in the *FSP* system.

In Fig.8 we show the charge and spin densities of the complete multiplet at  $\alpha = 100 \text{ meV} \cdot \text{\AA}$ ,  $U = 13 \text{ meV}$  and  $B = B^*$ . The situation is quite peculiar: by looking at  $\langle S_z \rangle$  [middle panel], we see that the GS has an up spin density everywhere in the dot, except for a tiny little reversed tail at the boundary. By contrast, the state  $J_z = 15/2$  has a down spin density at any  $r$ . Intermediate between the two, the *SKD* state displays a reversed spin at the center of the dot but the spin polarization changes into up when approaching the edge, to restore the spin density of the  $25/2$  state. There is a node in the middle. The other states ( $17/2, 19/2$  and  $21/2$ ) are rather featureless and they do not share these features. The trend is confirmed by looking at the projection of the spin density in the plane of the dot  $S_r = \hat{r} \cdot \vec{S}$  (see Fig.8[bottom panel]). This is the complementary information w.r. to  $S_z(r)$ . When  $S_r(r)$  is strongly non zero, then  $S_z(r)$  is heavily reduced.

An analogous interpolation occurs for the charge density. There is a piling up of the charge at the origin (see Fig.8[top panel]), corresponding to a locally dominant down spin density. The  $|SKD\rangle$  state is a collective excitation of the QD, which we call a “spin exciton”. In the next Section we show that the spin exciton recalls the first excited state of a *QHF* with some important differences, though.

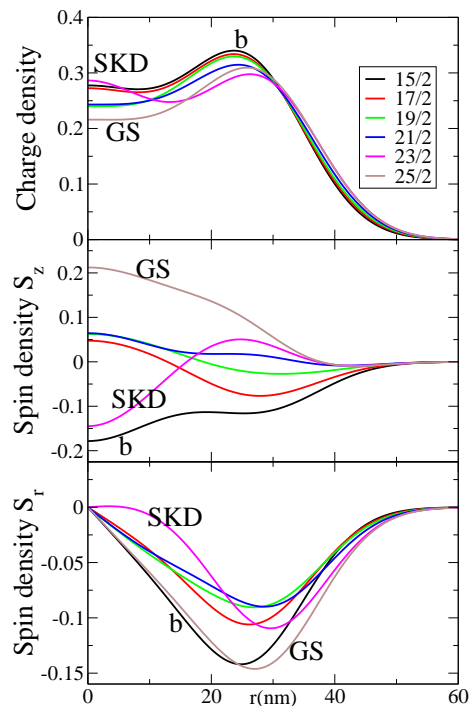


FIG. 8: (color on line) Charge density, azimuthal spin density  $S_z$ , in plane spin density  $S_r$ , in the radial direction, at various  $J_z$ . From bottom to top:  $J_z = 25/2$ (GS),  $23/2$ (SKD),  $21/2, 19/2, 17/2, 15/2$ . Other parameters are  $\alpha = 100 \text{ meV} \cdot \text{\AA}$ ,  $U = 13 \text{ meV}$  and  $\omega_d = 5 \text{ meV}$

## V. COMPARISON BETWEEN THE DOT AND A QHF DISK

The case of the dot in the *FSP* state can be compared with that of a disk shaped Quantum Hall Ferromagnet at filling one. The comparison is in order, because the physics of the dot turns into that of a quantum Hall disk by increasing the magnetic field, as long as the ratio  $\omega_d/\omega_c \rightarrow 0$ . Of course, while the infinite quantum Hall system is marked by a phase transition to the spin polarized state, the dot, being a system with a finite number of particles, undergoes a crossover to the *FSP* state which is not a broken symmetry state. This is confirmed by the presence of the tiny minority spin tail at the edge of the dot.

In the Subsection V.A, we recall some properties of the Hartree Fock description of the GS and first excited state of the QHF, which applies to filling close to (but less than) one.

Similarly, some analytical approximations leading to a simplified  $H - F$ -like approach for the dot with *SO* coupling will be discussed in Subsection V.B to highlight the analogies between the two systems.

### A. Quantum Hall Ferromagnet

In describing the QH state on a disk it is customary to label one particle states with  $\nu = (n - |m|)/2$  and  $m, \sigma$ , corresponding to the eigenvalues  $\epsilon_{\nu, m, \sigma}$  given in Eq.(3). The LLL includes the wavefunctions  $\phi_{nm}$  given by Eq.(1) for  $\nu = 0$  and  $m \geq 0$ . In this case all Laguerre polynomials  $L_0^{|m|}(t) = 1$ . If there is no confinement potential ( $\omega_d = 0$ ), all  $\epsilon_{0m}$  are degenerate. We rename the LLL wavefunctions  $f_{0m}\chi_\sigma$  (here  $\chi_\sigma$  denotes the spin 1/2 wavefunction) and associate the single particle fermion operators  $\hat{a}_{\nu=0m\sigma}$  to them. In the *QHF* at filling one, the LLL subband with, say, spin up, is fully occupied: the GS is a fully polarized spin state:

$$|QHF, 0\rangle = \prod_{0 \leq m \leq N-1} \hat{a}_{0m\uparrow}^\dagger |vac\rangle \quad (7)$$

Here  $|vac\rangle$  is the vacuum state. The lowest lying branch of excitations of the QHF are spin waves. These involve electrons in the down spin LLL subband and holes in the up spin LLL subband.

It was pointed out long ago<sup>28</sup> that, if the filling is slightly less than one, the first excited state can be a very special collective excitation with  $S < N/2$  and an extra node in the spin density. The spin polarization is reversed at the center, but gradually heals to the dominant spin background over a distance of many magnetic lengths (*SK* state). This excitation can be traced back to the *skyrmion*, the topological excitation of the  $O(3)$  *NLSM* in  $2-d$ <sup>23</sup>. A disk of infinite radius in coordinate space can be compactified to a sphere  $S^2$  in  $\mathcal{R}^3$  having the origin in the south pole and the point at infinity in the north pole. A similar compactification can be performed in the order parameter configurational space. An uniform magnetization “up” is represented by a vector pointing to the north pole everywhere on  $S^2$ . The skyrmion is a finite action configuration on  $S^2$ , satisfying the classical eq.s of motion for the magnetization of the *NLSM*, conserving  $\vec{J} = \vec{S} + \vec{M}$  and belonging to a non trivial homotopy class. If the topological charge is  $Q = 1$ , the shape of the magnetization field is  $\vec{s}(\vec{r}) = \hat{r}$ , where  $\hat{r}$  is the normal to  $S^2$  at each point.  $Q$  is the flux of  $\vec{s}(\vec{r})$  through the sphere of unit radius. The spin polarization is “down” at the south pole and turns over continuously in space, until it reaches “up” at the north pole. That is, the spin polarization is flipped at the origin of the disk w.r.to the GS and turns smoothly over away from it in the radial direction.

Within Hartree-Fock<sup>29</sup>, the Slater determinant  $|S, K\rangle$  that describes this state conserves total  $J_z$ . To construct it, a canonical transformation is performed on the fermion operators:

$$\begin{aligned} \hat{q}_j &= u_j \hat{a}_{0j-\frac{1}{2}\uparrow} + v_j \hat{a}_{0j+\frac{1}{2}\downarrow}, & j \in (\frac{1}{2}, \dots, \infty) \\ \hat{p}_{-\frac{1}{2}} &= \hat{a}_{00\downarrow} \\ \hat{p}_j &= -v_j \hat{a}_{0j-\frac{1}{2}\uparrow} + u_j \hat{a}_{0j+\frac{1}{2}\downarrow}, & j \in (\frac{1}{2}, \dots, \infty), \end{aligned} \quad (8)$$

Normalization requires that  $|u_j|^2 + |v_j|^2 = 1$ . Note that the operator  $\hat{p}_{-\frac{1}{2}}$  still belongs to the LLL as it destroys a particle in the  $f_{\nu=0, m=0}\chi_\downarrow$  state. We denote by  $f_j^{p/q}$  the single particle orbitals corresponding to the operators of Eq.(8) and we use them in Appendix A.

The generic Slater determinant built by means of these operators is:

$$|S, K\rangle = \prod_{j=\frac{1}{2}}^{\infty} \left( \hat{p}_{j-1}^\dagger \right)^{n_{j-1}^p} \left( \hat{q}_j^\dagger \right)^{n_j^q} |vac\rangle \quad (9)$$

$n_j^\beta$  are the occupation numbers of the single particle states ( $n_j^p = \langle p_j^\dagger p_j \rangle, n_j^q = \langle q_j^\dagger q_j \rangle$ ), with  $\sum_j n_j^\beta = N$ . The state of Eq.(9) is labeled by the total spin  $S$  and by  $K$ .  $S_z$  is no longer a good quantum number and is substituted by

$$K = S - \frac{1}{2} \sum_{j=\frac{1}{2}}^{N/2} (n_j^q - n_{j-1}^p) \quad (10)$$

The state of Eq.(9) with  $S = N/2, K = 0$  is the *FSP QHF* ground state of Eq.(7), if the only non zero occupation numbers are  $n_j^q = 1$  for  $j \in (\frac{1}{2}, \dots, N/2)$  with  $u_j = 1$  for  $j \in (\frac{1}{2}, \dots, N/2)$ . This state corresponds to the *FPS* GS of Fig.1b) for the QD case.

For the hard core model the HF equations can be solved analytically<sup>29</sup>. The lowest lying skyrmion state is  $|N/2, 1\rangle$ , with

$$|u_j|^2 = 1 - |v_j|^2 = \frac{\xi^2}{\xi^2 + (j + \frac{1}{2})} \quad (11)$$

leading to the spin density  $\vec{s}(\vec{r})$  defined in terms of the arbitrary length scale  $\xi$  ( $r^2 = x^2 + y^2$ )<sup>24</sup> (see Appendix):

$$s_x(\vec{r}) = \frac{2x\xi}{r^2 + \xi^2}; \quad s_y(\vec{r}) = \pm \frac{2y\xi}{r^2 + \xi^2}; \quad s_z(\vec{r}) = \frac{r^2 - \xi^2}{r^2 + \xi^2}. \quad (12)$$

The  $\pm$  refer to the sign of the topological charge  $Q = \pm 1$ . In the real *QHF* the length  $\xi$  is governed by the relative strength of the Zeeman and the Coulomb energies.

### B. Dot with spin-orbit coupling

In this Subsection we give arguments supporting our claim that the state *SKD* of Section IV corresponds to the state  $|N/2, 1\rangle$  in the *QHF* limit, that is in the limit of zero confinement potential and filling one. Indeed, the radial distribution of the spin density of the state *SKD* recalls the one of Eq.(12) except for a very shallow tail at the boundary. Away from the center the spin polarization of the *SKD* state lines up gradually with the one of the GS as it happens for the case of the Skyrmion. As in the *SK* case,  $S_z(r)$  has an extra node at  $r = \xi$ . In the

presence of  $SO$ , the length scale  $\xi$  is no longer arbitrary, but is fixed by the strength of the  $SO$  coupling.

In the case of the  $QHF$  on a disk, both rotations in real space around the  $z$ -axis and rotations in spin space are good symmetries, so that  $M$  as well as  $S_z$  are conserved. This implies that an allowed  $SK$ -like excited state of the real system has to be obtained by projecting the state of Eq.(9) onto the subspace of definite  $M$  and  $S_z$ . This is not necessary in the QD with  $SO$  interaction, because the  $SO$  hamiltonian term only conserves  $J_z$  as the state  $|S, K\rangle$  does. In the following we show that a simplified  $H - F$ -like approach for the dot case with  $SO$  coupling shows features similar to the ones described by Eq.s (8), (11) and Eq.s (9), (12). Let us first discuss  $SO$  coupling in the dot at  $U = 0$ . The vector space required to diagonalize the  $SO$  coupling and to obtain the eigenfunctions  $w_{j_z}^\beta$  exceeds the LLL space enormously (in practice we always use the basis of Eq.(1) and never calculate the  $w_{j_z}^\beta$ 's explicitly). As a simple analytical approximation, we can restrict ourselves to the LLL for sake of simplicity. We have checked numerically that this approximation is largely satisfactory away from the level crossings. In this case, diagonalization of the  $SO$  interaction factorizes the problem into a collection of  $2 \times 2$  matrices. What the  $SO$  does is to mix single particle states with different  $m$  and opposite spins in the way that the transformation of Eq.(8) shows. Indeed,  $j_z$  ( $j_z \equiv j$  in the following) is conserved. Within the LLL, two  $(m, \sigma)$  values contribute to each half integer  $j$ :  $(m, \uparrow)$  and  $(m + 1, \downarrow)$ . The unperturbed energy levels involved,  $\epsilon_{0m}$  and  $\epsilon_{0m+1}$ , are given by Eq.(3). Let the offdiagonal matrix element including the  $SO$  coupling be  $\alpha$ . Then the eigenvalues are:

$$\lambda_j^{p/q} = \frac{1}{2}(\epsilon_{0m} + \epsilon_{0m+1}) \pm \sqrt{\frac{\delta^2}{4} + \alpha^2}, \quad (13)$$

where  $\delta = \epsilon_{0m+1} - \epsilon_{0m} = \omega_o - \omega_c/2$ . The diagonalization implies a rotation in the 2-vector space  $\{f_{0m}\chi_\uparrow, f_{0m+1}\chi_\downarrow\}$  of an angle  $\gamma$  given by  $\tan 2\gamma = -2\alpha/\delta$ . The single particle states obtained in this way coincide with  $f_j^{p/q}$  defined after Eq.(8). The mixing of the two states  $(m, \uparrow)$  and  $(m + 1, \downarrow)$  is  $j$ -independent, within our approximations, because  $\delta$  is. This implies that the rotation angle  $\gamma$  keeps roughly constant in the radial direction, because average radial distribution of an electron of angular momentum  $j$  is  $\sim l\sqrt{j+1}$ . We can now construct the Slater determinants representing the states lower lying in energy. The states corresponding to the ones obtained numerically in Section IV are depicted in Fig.(9). In analogy to Fig.(1) we use boxes to allocate electrons. Each box is cut into a lower and an upper triangle w.r.to the diagonal, corresponding to the  $q$  and the  $p$  state of a given  $j_z$ , respectively. A dot marks which of the orbitals is occupied. We have analyzed the Slater determinants which contribute mostly to the states obtained at the end of the Lanczos procedure, giving the average occupation numbers of Fig.(7). Their largest components indeed contain the determinants shown in

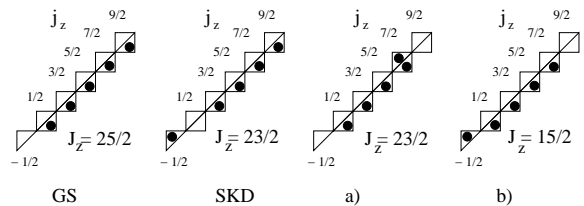


FIG. 9: Slater determinants quoted in the text with the same labels. Quantum numbers are  $N = 5$ ,  $S = 5/2$  and  $J_z$ . Upper/ lower triangle refer to single particle states labeled by  $j_z$  and  $p/q$ . Other possible quantum numbers do not appear. The dots mark occupied states. Configuration labeled as a) is involved in a state belonging to a much higher energy.

Fig.(9).

There is close similarity with the results of Subsection V.A. However a relevant difference can be immediately recognized. While the skyrmion shows a very smooth tilting of the spin orientation with increasing distance from the center of the disk (see Eq.(11)), the rotation angle  $\gamma$  for the dot is uniform in the radial direction. This feature is partly compensated by the addition of the Coulomb repulsion. Indeed,  $U \neq 0$  predominantly affects the occupations close to the center of the dot disk, while its influence fades out away at larger distances. This fact introduces a radial variation of the tilting of the spin polarization. According to Eq.(12), the skyrmion has a linear variation with radial distance of  $S_r$ , close to the origin. By contrast, our numerical results reported in Fig.(5 [bottom panel]) show a quadratic increase at small  $r$ 's.

The role of  $U$  is quite substantial, by locating the energy of the  $SKD$  state intermediate between those of the  $GS$  and of the  $b$  state. Needless to say, another relevant and obvious difference between  $SKD$  and  $SK$  is the absence of any conserved topological charge in the dot. In the  $QHF$  the conservation of  $Q$  is implemented on symmetry grounds, by mapping the QH disk onto a sphere. This mapping cannot be extended to the dot, because, as seen from Fig.(8), the direction of the magnetization at the boundary is not unique. Magnetization is not defined at  $\vec{r} \rightarrow \infty$ : the point at infinity is a singular point in the magnetization configurational space.

## VI. CONCLUSIONS

In a disk shaped quantum dot with few electrons, interactions drive the system to a fully spin polarized state with  $S = N/2$ , in the presence of a magnetic field  $B = B^*$  orthogonal to the dot. At  $B > B^*$ , the total spin is again drastically reduced and the charge density reconstructs at the disk boundary. We have reported on exact diagonalization results of a QD with  $N = 5$  electrons and studied the effect of  $SO$  coupling possibly due to an external electric field orthogonal to the dot disk. There are analogies between the dot state at  $B = B^*$  and the



Quantum Hall Ferromagnet at filling one. We require a sizeable interaction strength  $U$  to stabilize the  $FSP$  GS. When the  $SO$  coupling is increased, level crossings occur in the splitted  $S = 5/2$  multiplet, until the state with maximum  $J_z = M + S_z = 25/2$  becomes the GS. The first excited state ( $SKD$  state) has  $J_z = 23/2$ . When compared to the GS, the  $SKD$  state has some charge transferred to the dot center and a very peculiar spin texture. Indeed, the  $z$ -component of the spin density at the center of the dot is opposite to the one of the GS and rotates continuously over away from the center, by acquiring the same profile as the one of the GS at the dot boundary. This winding requires an extra node in the spin density, which is absent in the other multiplet states. According to these properties, the  $SKD$  state can be viewed as carrying one spin exciton. Both our numerical results of Section III-IV, and our approximate analytical speculation of Section V show how essential the combined role of the  $SO$  coupling and of the  $e-e$  interaction is in stabilizing this state. Our calculation parametrizes the interaction strength  $U$ , but it ignores the screening of the  $e-e$  interaction altogether. This should be reconsidered in view of the fact that vertical QD's are separated on the top and the bottom from the contact metals by barriers with a typical width of  $70\text{\AA}$ . Even for  $N = 5$  this is smaller than the inter-electron spacing<sup>30</sup>. However, we believe that the exciton state is robust when the screening is included. Indeed, the flipping of the spin is concentrated at the center of the dot and is governed by the  $e-e$  interaction at short range, which should be largely insensitive of screening effects. The  $SKD$  state recalls the skyrmion excitation which takes place in a disk shaped  $QHF$  at filling one. The statement could be puzzling, in view of the fact that the  $SO$  coupling is essential to the  $SKD$  state, but it is never invoked when discussing Quantum Hall properties. However field theory models ( $NL\sigma M$ ) use the conservation of  $J$  to prove the existence of the skyrmion state. In a real isolated QH disk  $M, S_z$  would keep finite and separately conserved. In this case only the component of the  $SK$  state that conserves given values of  $M, S_z$  would be present in the excitation spectrum. Nonetheless the difference is washed out in the limit of an infinite disk size. This is the continuous limit which leads to the  $NL\sigma M$ . In the case of the dot, the compactification of both the coordinate space and the magnetization space cannot be performed because the direction of the magnetization is not defined at  $\vec{r} \rightarrow \infty$ . Therefore no state can be constructed that conserves  $J_z$  only, without conserving  $M$  and  $S_z$  separately. The spin orbit coupling opens up this possibility. However, no topological charge can be associated to the  $SKD$  state in the dot.

Our calculation shows that for realistic values of the dot confining potential ( $\omega_d = 5meV$ ), of the Coulomb interaction strength ( $U = 13meV$ ) and of the  $SO$  coupling  $\alpha \sim 100meV\text{\AA}^{31}$ , the  $FSP$  GS and the  $SKD$  state are well spaced levels. The other levels of the multiplet appear at higher energies and are rather close to each other.

This means that, at  $B = B^*$ , the dot opens a sizeable spin gap between the GS and the  $SKD$  state, that can be tuned with an applied gate. This spin gap cannot be washed out by thermal fluctuations, if the temperature is low enough ( $\sim 50mK$ ). The gap can be probed by optically pumped NMR as in quantum wells<sup>22</sup>. Spin-lattice relaxation of  $^{71}Ga$  nuclear spins in the dot, driven by the hyperfine coupling to the dot electrons should be very much reduced, thus leading to a large  $T_1$ .

The extremely low spin relaxation expected for this excitation, could allow for a coherent manipulation of the spin exciton using terahertz radiation<sup>35,36,37</sup>. In general, we believe that the system studied here can be relevant to the coherent manipulation of QD states. This is appealing in view of quantum information processing<sup>32,33,34</sup>. Indeed, a spectrum like the one calculated in this work should produce sharp optical absorption lines. Photoluminescence induced by a pump and probe laser technique has been studied in disk shaped  $InGaAs$  QD's with evidence for Rabi oscillations<sup>38</sup>. In our case, because of the presence of  $B$ , a circularly polarized pulse of one single chirality can excite the spin exciton discussed here.

### Acknowledgments

The authors acknowledge important discussions with B. Altshuler, S. De Franceschi, P. Onorato, D. Zumbuhl.

### APPENDIX A: QHF SPIN DENSITY

In this appendix we show that the state  $|N/2, 1\rangle$  given by Eq.(9) with  $u_j$  given by Eq.(11) leads to the skyrmion spin density of Eq.(12).

The wavefunctions for the QH disk associated to the operators  $\hat{a}_{0m\sigma}$  are given in Eq.(1). In the LLL ( $\nu = (n - |m|)/2 = 0$ ) all Laguerre polynomials  $L_0^m(t) = 1$ . To construct the field operator, we associate a spinorial wavefunction  $f_j^{p/q}(\vec{r})$  to the operator  $\hat{p}_j/\hat{q}_j$  following Eq.(8):

$$f_j^p(\vec{r}) = \begin{pmatrix} -v_j f_{0j-\frac{1}{2}}(\vec{r}) \\ u_j f_{0j+\frac{1}{2}}(\vec{r}) \end{pmatrix}, \quad j \in (\frac{1}{2}, \dots, \infty) \quad (A1)$$

and analogously for  $f_j^q$ . We take  $u_j$  and  $v_j$  real. The field operator is:

$$\hat{\psi}(\vec{r}) = \sum_{j=\frac{1}{2}}^{\infty} (f_{j-1}^p(\vec{r})\hat{p}_{j-1} + f_j^q(\vec{r})\hat{q}_j) . \quad (A2)$$

The spin density operator is  $\hat{s}(\vec{r}) = \Re \left\{ \hat{\psi}^\dagger(\vec{r}) \vec{\sigma} \hat{\psi}(\vec{r}) \right\}$ , to be evaluated on the state  $|N/2, 1\rangle$ . Let us consider  $s_x(\vec{r})$  first. The term including the  $\hat{p}_j$  operators does not contribute, because all the  $f^p$  orbitals are unoccupied in the state  $|N/2, 1\rangle$ , except for  $j = -\frac{1}{2}$ . On the other hand this term, does not appear, because  $u_{-\frac{1}{2}} \cdot v_{-\frac{1}{2}} \equiv 1 \cdot 0 = 0$ .

The contribution to  $s_x(\vec{r})$  given by the  $\hat{q}_j$  operators is:

$$\sum_{j=\frac{1}{2}}^{\infty} \begin{pmatrix} u_j f_{0j-\frac{1}{2}}^*(\vec{r}) & v_j f_{0j+\frac{1}{2}}^*(\vec{r}) \\ v_j f_{0j-\frac{1}{2}}^*(\vec{r}) & u_j f_{0j+\frac{1}{2}}^*(\vec{r}) \end{pmatrix} \begin{pmatrix} 0 & 1 \\ 1 & 0 \end{pmatrix} \begin{pmatrix} u_j f_{0j-\frac{1}{2}}(\vec{r}) \\ v_j f_{0j+\frac{1}{2}}(\vec{r}) \end{pmatrix} \\ = \sum_{j=\frac{1}{2}}^{\infty} 2u_j v_j f_{0j-\frac{1}{2}}^*(\vec{r}) f_{0j+\frac{1}{2}}(\vec{r}) \quad . \quad (\text{A3})$$

Using Eq.(11) we get  $(\vec{r} \equiv (r, \varphi))$ :

$$2\xi \sum_{j=\frac{1}{2}}^{\infty} \Re \left\{ e^{i\varphi} \frac{r^{j-\frac{1}{2}} r^{j+\frac{1}{2}}}{(j-\frac{1}{2})!^{\frac{1}{2}} (j+\frac{1}{2})!^{\frac{1}{2}}} \frac{(j+\frac{1}{2})^{\frac{1}{2}}}{\xi^2 + (j+\frac{1}{2})} e^{-r^2} \right\} \\ = 2\xi \quad r \cos \varphi \sum_{j=\frac{1}{2}}^{\infty} \frac{(r^2)^{j-\frac{1}{2}} e^{-r^2}}{(j-\frac{1}{2})!} \frac{1}{\xi^2 + (j+\frac{1}{2})} . \quad (\text{A4})$$

Because the maximum of the first factor occurs for  $j+\frac{1}{2} \sim r^2$  we evaluate the denominator of the second factor by substituting  $j+\frac{1}{2} \rightarrow r^2$ , what allows us to perform the sum explicitly. By noting that  $r \cos \varphi = x$  we obtain  $s_x(\vec{r})$  as given by Eq.(12). A similar calculation applies for  $s_y(\vec{r})$ . In the case of  $s_z(\vec{r})$ , the extra factor is  $v_j^2 - u_j^2 = [(j+\frac{1}{2}) - \xi^2]/[(j+\frac{1}{2}) + \xi^2]$  and  $\varphi$  disappears. Using the same approximations as above, we obtain the result of Eq.(12).

- 
- <sup>1</sup> L.P. Kouwenhoven, D.G. Austing, S. Tarucha Rep. Prog.Phys. **64** (6), 701-736 (2001); L.P. Kouwenhoven and C.M. Marcus Phys. World **116**, 35-39 (1998); M.A.Kastner, Ann.Phys.(N.Y.) **9**, 885 (2000).
  - <sup>2</sup> L.Jacak, P.Hawrilack, A.Wójs, Quantum Dots, Springer-Verlag Berlin (1998).
  - <sup>3</sup> S. Tarucha, D. G. Austing, T. Honda, R. J. van der Hage, and L. P. Kouwenhoven, Phys. Rev. Lett. **77**, 3613 (1996).
  - <sup>4</sup> Y.Ishikawa and H. Fukuyama, Journ. of Phys. Soc. Japan **68**(7), 2405 (1999).
  - <sup>5</sup> This is due to the fact that the hamiltonian term coupling  $B_{\perp}$  to  $M$  is  $\mu_B^* B_{\perp} M$  where  $\mu_B^* = e\hbar/2m^*c$  is the effective Bohr magneton ( $m^*$  is the effective mass). On the other hand the Zeeman spin splitting term is  $g^* \mu_B B_{\perp} S_z$ , where  $g^*$  is the effective gyromagnetic factor for electrons in this geometry (very low in many semiconductor heterostructures) while  $\mu_B$  is the Bohr magneton with the bare mass (spin is insensitive to band effects). The situation is similar to what happens in the QHE where  $\omega_c$  includes the effective mass and Landau level separation is increased by a factor of  $\sim 20$ , while Zeeman spin splitting, being reduced by a factor of 4, becomes negligible in comparison. (A.H.MacDonald, in NATO ASI: 'Quantum transport in semiconductor submicron structures', B.Kramer ed.(Kluwer Berlin, 1996))
  - <sup>6</sup> W.G. van der Wiel et al., Physica B **256**, 173 (1998).
  - <sup>7</sup> T.Schmidt et al., Phys.Rev.B **51**,5570 (1995).
  - <sup>8</sup> H.Imamura, H.Aoki, and P.A.Maksym, Phys.Rev.B **57**,R4257 (1998); D. Weinmann, W. Häusler, and B. Kramer, Phys. Rev. Lett. **74**, 984 (1995).
  - <sup>9</sup> B.Jouault, G.Santoro, A.Tagliacozzo, Phys.Rev.B **61**, 10242 (2000).
  - <sup>10</sup> I.L. Aleiner, P.W. Brouwer and L.I. Glazman, Phys. Rep. **358**, 309 (2002).
  - <sup>11</sup> D.Giuliano, B.Jouault, A.Tagliacozzo, Europhys. Lett. **58**, 401 (2002).
  - <sup>12</sup> D. Giuliano, P. Sodano, A. Tagliacozzo, Phys. Rev. B **67**, 155317 (2003).
  - <sup>13</sup> O.Klein et al., Phys.Rev.Lett **74**, 785(1995); O.Klein et al., Phys.Rev.B **53**,4221(1996).
  - <sup>14</sup> T.H.Oosterkamp, et al., Phys.Rev.Lett. **82**, 2931, (1999).
  - <sup>15</sup> L.P.Rokhinson, L.J. Guo, S.Y. Chou and D.C. Tsui, Phys.Rev.Lett. **87**, 166802 (2001).
  - <sup>16</sup> C.de Chamon and X.G.Wen, Phys.Rev.B **49**, 8227 (1994); S.M.Reimann, M.Koskinen, M.Manninen, B.R.Mottelson, Phys.Rev.Lett.**83**,3270 (1999).
  - <sup>17</sup> for a review see: S.M.Reimann and M.Manninen, Rev.Mod.Phys. **74**, 1283 (2002).
  - <sup>18</sup> D.Pfannkuche, V.Gudmundsson, and P.A.Maksym, Phys.Rev.B **47**, 2244 (1993).
  - <sup>19</sup> M.Stopa, Phys.Rev.B **54**, 13767 (1996).
  - <sup>20</sup> R.Egger, W.Häusler, C.H.Mak, and H. Grabert Phys. Rev. Lett. **82** 3320 1999; R.Egger, W.Häusler, C.H.Mak Phys. Rev. Lett. **83** 462 1999.
  - <sup>21</sup> E.I.Rashba, Fiz. Tverd. Tela **2**, 1224 (1960) [Sov.Phys. - Solid State **2**, 1109 (1960), Y.A.Bychkov, E.I.Rashba, J.Phys.C**17**, 6039 (1984).
  - <sup>22</sup> R.Tycko et al., Science **268**, 1460 (1995).
  - <sup>23</sup> A.A.Balavin and A.M.Polyakov, JETP Lett.**22**, 245(1975); A.M.Polyakov, Phys.Lett. **59B**, 79 (1975).
  - <sup>24</sup> R.Rajaraman *Soliton and instantons*, North Holland, Amsterdam (1982).
  - <sup>25</sup> E.H.Aifer, B.B.Goldberg and D.A.Broido, Phys. Rev. Lett. **76**, 680(1996)
  - <sup>26</sup> M.Abramowitz, I.A.Stegun, Handbook of Mathematical Functions with Formulas, Graphs and Mathematical Tables, Dover (New York 1972).
  - <sup>27</sup> A.Karlhede et al., Phys.Rev.Lett.**77**, 2061 (1996).
  - <sup>28</sup> B.I.Halperin, Helv.Phys. Acta **56**,75 (1983)
  - <sup>29</sup> H. A. Fertig et al., Phys.Rev.B **55**, 10671 (1997) ; M.Abolfath et al., Phys.Rev.B **56**, 6795 (1997);
  - <sup>30</sup> We indebted to the referee for this remark.
  - <sup>31</sup> In *In Ga As*  $\alpha$  is about  $70 meV \text{ \AA}$  at zero electric field. It can be increased by applying a gate voltage. (J.Nitta, T.Akazaki, H.Takayanagi and T.Enoki, Phys. Rev. Lett, **78** ,1335 (1997); D.Grundler, Phys. Rev. Lett. **84**, 6074 (1999)).
  - <sup>32</sup> P.Chen,C.Permarocchi and L.J.Sham, Phys. Rev. Lett.**87**, 067401 (2001).
  - <sup>33</sup> G.Chen et al., Science **289**, 1906 (2000).
  - <sup>34</sup> N.H.Bonadeo et al., Science **282** , 1473 (1998).
  - <sup>35</sup> T.Takagahara J. of Luminescence **87-89**, 308 (2000).
  - <sup>36</sup> D.D.Awshalom, J.M.Kikkawa, Phys.Today. **52**, 33 (1999).
  - <sup>37</sup> B.E.Cole et al., Nature **410**,60 (2001).

<sup>38</sup> H.Kamada et al., Phys. Rev.Lett.**87**,246401 (2001).